Proceedings of "Applications of Physics in Mechanical and Material Engineering" (APMME 2023)

Numerical Investigations of the Influence of Cooling Rate During Solidification on Shrinkage Cavities and Grain Formation Process

T. Skrzypczak*, E. Węgrzyn-Skrzypczak and L. Sowa

[a] *Czestochowa University of Technology, 42-201 Częstochowa, Poland*

Doi: 10.12693/APhysPolA.144.342 *e-mail: tomasz.skrzypczak@pcz.pl

The presented work focuses on the numerical modeling of the solidification process, with a particular emphasis on two significant physical phenomena: shrinkage cavities and grain formation, which are influenced by the cooling rate. Cooling rate plays a crucial role in determining grain size and casting defects. Higher cooling rates result in finer grain structures, while slower rates promote larger grains. During solidification, atoms arrange into crystalline structures, forming grains. The cooling rate affects grain growth kinetics. Faster rates lead to smaller grains due to limited atomic diffusion, while slower rates allow for larger grain growth. Shrinkage cavities, localized regions in solidified material, form due to volume contraction during cooling, negatively impacting mechanical properties. In this paper, the main assumptions of the mathematical and the numerical model are presented. The numerical description of the problem is based on the finite element method, which is a widely used numerical technique for solving complex physical problems. The algorithm for the shrinkage cavity creation process is described, and an original computer program was developed using the numerical model. The computer simulation was conducted to obtain distributions of temperature, grain size, as well as the position and shapes of the shrinkage cavities.

topics: solidification, grain size, cooling rate, shrinkage cavity

1. Introduction

Technological processes such as casting involve the consideration of various thermal phenomena. Casting is a process where a liquid metal solidifies within a mold made of sand or cast iron. During this process, heat is transferred out of the casting. As the casting forms, the liquid and solid phases contract due to the cooling process. Additionally, shrinking occurs during the transformation of the material from the liquid to the solid state. The temperature decrease in different parts of the casting leads to contraction, which is the primary cause of the formation of micro- and macroscopic defects. Cone-shaped open voids observed at the top of the riser and closed voids located deeper within the solidifying system are the most frequently encountered macroscopic defects [1–2]. Extensive discussions on numerical models concerning the formation of shrinkage defects can be found in the literature [3–11]. Books [3, 4] provide fundamental insights into the formation of shrinkage cavities during casting solidification. In one particular study [5], the focus lies on predicting the distribution of defects in a casting with a simple shape. As computational power has increased, researchers have been able to model the formation of shrinkage cavities in three-dimensional spaces [6–11]. This has been achieved using proprietary software [6] as well as commercially available software [7–11]. These models also consider additional factors such as porosity formation [8] and the macrosegregation of components [7, 9, 10].

The cooling rate of the casting has a significant impact on the formation of its primary structure. The primary structure of the casting refers to the arrangement of crystals that form during the material solidification process. The cooling rate determines the solidification rate and affects the size and distribution of crystals within the casting. Fast cooling promotes rapid solidification, resulting in a fine-grained primary structure. A shorter solidification time means that the crystals have less time to grow, resulting in smaller grain sizes. A fine-grained primary structure exhibits higher mechanical strength, a harder surface, and improved resistance to cracking. On the other hand, slow cooling leads to a slower solidification process and the formation of a coarse-grained primary structure. A longer solidification time allows the crystals to grow more extensively, resulting in larger grain sizes. A coarse-grained primary structure may have lower mechanical strength, a less hard surface, and increased susceptibility to cracking. The cooling rate has a significant influence on the size of the frozen crystal zone, columnar crystal zone, and equiaxed grain zone.

2. Mathematical and numerical description

In the analysis, a solidifying casting with a riser is taken into account (see Fig. 1). Heat transfer through the casting's side and top surfaces is incorporated through appropriate boundary conditions. The region under consideration is divided into several zones based on the amount of liquid, solid, and gas present. The primary domains of the solidifying casting include the solid region Ω_S, the liquid region Ω_L, and the region Ω_A filled with air. Additionally, during the solidification process, the solid-liquid area Ω_{S+L} is also observed. The outer boundaries of the analyzed casting are the side surface Γ_{side} and the top surface Γ_{top}. Due to symmetry, only half of the system was considered, which also involved the introduction of a symmetry plane Γ_{sym}.

The problem's mathematical description includes the transient heat transfer partial differential equation

$$\nabla \cdot (\lambda \nabla T) = c\rho \frac{\partial T}{\partial t} \tag{1}$$

and encompasses the related boundary-initial conditions

$$(x, y, z) \in \Gamma_{top}, \Gamma_{side}: \quad -\boldsymbol{n} \cdot \lambda \nabla T = \alpha (T - T_\infty), \tag{2}$$

$$(x, y, z) \in \Gamma_{sym}: \quad -\boldsymbol{n} \cdot \lambda \nabla T = 0, \tag{3}$$

$$T(x, y, z, t{=}0) = T_0. \tag{4}$$

The symbols in this context hold the following meanings: λ [J/(s m K)] represents the coefficient of thermal conductivity, T [K] denotes the temperature. The effective specific heat parameter c [J/(kg K)] describes the release of heat during solidification. The density ρ [kg/m^3] determines the mass per unit volume. The variable t [s] signifies time, while $\boldsymbol{n}$ denotes the normal vector to the external boundaries Γ_{side} and Γ_{top}. The heat transfer coefficient α [J/(s m^2 K)] represents the convective heat transfer outside Γ_{side} and Γ_{top}, respectively. Next, T_0 [K] represents the initial temperature distribution, and T_∞ [K] corresponds to the temperature of an external medium, such as a mold or air. Lastly, ∇ symbolizes the Nabla operator.

To determine the density ρ and the thermal diffusion coefficient λ, their average values can be computed using the following formulas

$$\begin{aligned} \rho &= f_S \rho_S + (1 - f_S)\rho_L, \\ \lambda &= f_S \lambda_S + (1 - f_S)\lambda_L, \end{aligned} \tag{5}$$

$$f_s = \frac{T_L - T}{T_L - T_S}, \tag{6}$$

$$\begin{cases} T < T_S: & c = c_S, \\ T_S \le T \le T_L: & c = \dfrac{c_L + c_S}{2} + \dfrac{L_H}{T_L - T_S}, \\ T > T_S: & c = c_L, \end{cases} \tag{7}$$

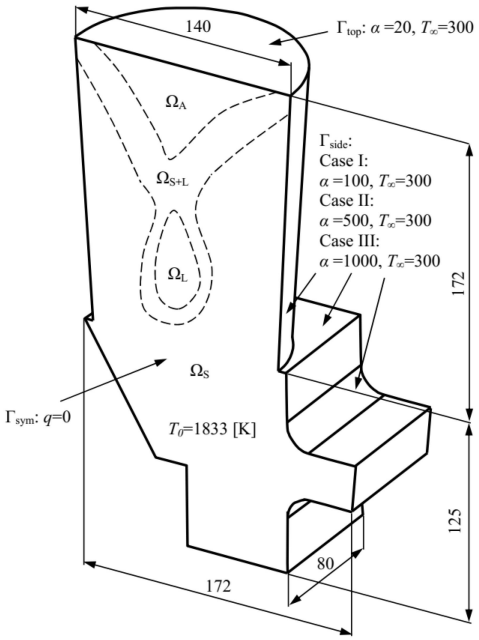

Fig. 1. Solidifying casting with marked characteristic zones and boundary-initial conditions. Dimensions in millimeters.

where f_S [-] represents the fraction of the solid phase, and T_L [K] and T_S [K] denote the liquidus and solidus temperature, respectively. The effective specific heat c (7) is expressed in reference [12]. The subscripts L and S denote the liquid and solid phases, respectively, and L_H [J/kg] signifies the latent heat of solidification. The numerical model is built using the finite element method (FEM), where (1) is employed along with the initial and boundary conditions (2)–(4). The weighted residuals criterion has been applied in formulating FEM,

$$\int_\Omega \mathrm{d}\Omega \; w \left[-c\rho \frac{\partial T}{\partial t} + \nabla \cdot (\lambda \nabla T) \right] = 0. \tag{8}$$

In the above equation, w is the test function, and Ω represents the total volume of the casting. Utilizing the standard Galerkin formulation, a set of equations is derived. Specifically, for each finite element (e), the following equation can be obtained

$$\begin{aligned} \lambda^{(e)} \int\int_{\Omega^{(e)}} \mathrm{d}\Omega \; \left(\boldsymbol{D}_x^{\mathrm{T}} \boldsymbol{D}_x + \boldsymbol{D}_y^{\mathrm{T}} \boldsymbol{D}_y + \mathrm{D}_z^{\mathrm{T}} \mathrm{D}_z \right) \boldsymbol{T} = \\ - \int_{\Gamma^{(e)}} \mathrm{d}\Gamma \; q\boldsymbol{N} - c^{(e)} \rho^{(e)} \int\int_{\Omega^{(e)}} \mathrm{d}\Omega \; \boldsymbol{N}^{\mathrm{T}} \boldsymbol{N} \dot{\boldsymbol{T}}. \end{aligned} \tag{9}$$

To compute the temperature distribution, the equation utilizes the shape functions $\boldsymbol{N}$ of the finite element, along with the spatial derivatives $\boldsymbol{D}_x$, $\boldsymbol{D}_y$, and $\boldsymbol{D}_z$ of the shape functions with respect to x, y, and z, respectively. The nodal values of temperature and its time derivatives are contained in $\boldsymbol{T}$. Additionally, the boundary heat flux is represented by q. The computation employs the backward Euler method for time discretization,

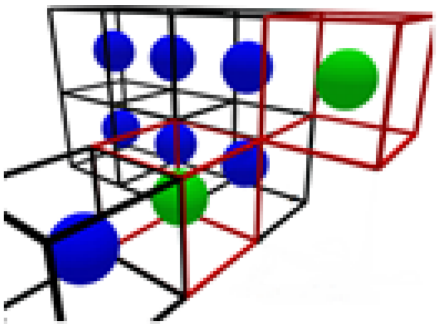

Fig. 2. Simplified structure of the mushy zone.

TABLE I

Material properties used in the calculations.

Material property	Liquid phase	Solid phase	Air
λ	23	35	0.3
ρ	6915	7800	1.0
c	837	644	1008.2
Parameter of solidification	Value		
L	270000		
T_L	1774.0		
T_S	1718		
S_h	0.05		
$d_{\max g}$	0.0002		

resulting in the following scheme

$$\left((\Delta t)^{-1}\boldsymbol{M}+\boldsymbol{K}\right)\boldsymbol{T}^{j+1}=\boldsymbol{B}+(\Delta t)^{-1}\boldsymbol{M}\boldsymbol{T}^{j}. \tag{10}$$

In this model, the assumption was made that the mushy zone comprises spherical grains that grow within a liquid matrix (see Fig. 2). It was also assumed that liquid flow between grains remains feasible until neighboring grains make contact with each other.

The size of the cell $d_{\max l}$ [m] in which the grain grows was calculated using the equation [13]

$$d_{\max l}=d_{\max g}\left(1-\mathrm{e}^{-1/CR}\right), \tag{11}$$

where $d_{\max g}$ [m] represents the maximum grain size that can form in the casting, and CR [K/s] denotes the cooling rate of solidification.

The critical value of the solid phase fraction at which fluid flow occurs in the mushy zone is $f_{skr}=0.52$, based on the assumption made

$$f_{skr}=\frac{V_{grain}}{V_{cell}}=\frac{4\pi}{3}\left(\frac{a}{2}\right)^3 a^{-3}=\frac{\pi}{6}=0.52. \tag{12}$$

The algorithm for shrinkage cavity growth consists of the following stages at each time step:

- Calculation of the increment of the solid phase based on the temperature field in the current and previous time steps.

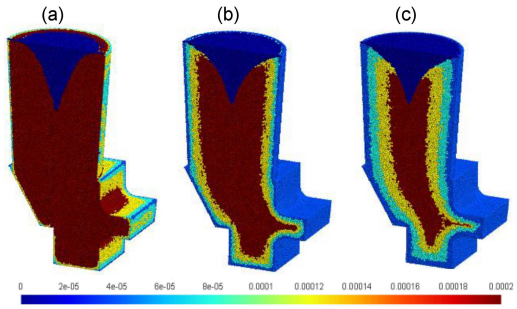

Fig. 3. Primary structure of the casting and location of the shrinkage cavity for cases I (a), II (b), and III (c).

- Computation of the material shrinkage by multiplying the volume of the solid phase by the shrinkage coefficient S_h [-].
- Assigning the calculated volumetric loss to the highest located nodes in the corresponding liquid regions, changing their state from liquid (L) to air (A). This procedure forms one or more shrinkage cavities.

This process should be repeated at each time step until no L nodes remain in the casting.

3. Example of calculations

Three variants of calculations were performed for the geometry shown in Fig. 1. The geometry was modeled and spatially discretized using the open-source software Gmsh. The mesh was composed of tetrahedral elements and consisted of 95501 nodes. Each simulation case was conducted with a different cooling intensity on Γ_{side}, corresponding to a specified value of the coefficient α (Fig. 1). The time step was $\Delta t=0.1$ s. The material properties of steel are presented in Table I. The casting was initially filled with molten alloy at a temperature of 1833 K.

In Fig. 3, the structure of the casting after solidification is shown. It is evident that the cooling rate influences the location and extent of regions with different grain sizes. In the case of slow cooling, a zone dominated by equiaxed grains is observed (Fig. 3a), while in the case of intense cooling (Fig. 3c), frozen and columnar grain regions are visible, along with a central region occupied by the largest equiaxed grains. The shrinkage cavity exhibits a similar shape and depth in all three cases.

4. Conclusions

The cooling rate was found to have a significant influence on the primary structure of the casting. Different cooling rates resulted in varying proportions of frozen columnar and equiaxed grain regions.

Slow cooling led to the dominance of equiaxed grain regions, while intense cooling promoted the formation of frozen and columnar grain regions. The cooling rate did not have a substantial influence on the shrinkage cavity itself. Although there was a slight difference in depth, with a slightly deeper shrinkage cavity observed under slower cooling conditions, the overall shape and location of the shrinkage cavity remained relatively consistent across the different cooling rates.

References

[1] Ch. Pequet, M. Rappaz, M. Gremaud, *Metall. Mater. Trans. A* **33**, 2095 (2002).

[2] M. Bellet, O. Jaouen, I. Poitrault, *Int. J. Numer. Method. H.* **15**, 120 (2005).

[3] J. Campbell, *Castings*, 2nd ed., Butterworth-Heinemann, Oxford 2003.

[4] M.C. Flemings, *The solidification processing*, Mc Graw-Hill, New York 1974.

[5] C.J. Kim, S.T. Ro, *J. Heat. Trans.* **115**, 1078 (1993).

[6] A.S. Jabur, F.M. Kushnaw, *J. Appl. Computat. Math.* **6**, 7 (2017).

[7] A. Ludwig, M. Wu, A. Kharicha, in: *CFD Modeling and Simulation in Materials Processing 2016*, Springer 2016, p. 3.

[8] C. Zhang, Y. Bao, M. Wang, L. Zhang, *Arch. Foundry Eng.* **16**, 27 (2016).

[9] M. Wu, A. Ludwig, A. Kharicha, *Appl. Math. Model.* **41**, 102 (2017).

[10] M. Xie, H. Shen, *Front. Mater.* **7**, 13 (2020).

[11] K. Zheng, Y. Lin, W. Chen, L. Liu, *Adv. Mech. Eng.*, **12**, 1 (2020).

[12] B. Mochnacki, J.S. Suchy, *Numerical Methods in Computations of Foundry Processes*, Polish Foundrymen's Technical Association, Kraków 1993.

[13] N. Sczygiol, *Modelowanie Numeryczne Zjawisk Termomechanicznych w Krzepnącym Odlewie i Formie Odlewniczej*, Wydawnictwo Politechniki Częstochowskiej, Częstochowa 2000.